Mechanical regulation of cell function with geometrically modulated elastomeric substrates

Jianping Fu[1–3], Yang-Kao Wang[1–3], Michael T Yang[1], Ravi A Desai[1], Xiang Yu[1], Zhijun Liu[1] & Christopher S Chen[1]

We report the establishment of a library of micromolded elastomeric micropost arrays to modulate substrate rigidity independently of effects on adhesive and other material surface properties. We demonstrated that micropost rigidity impacts cell morphology, focal adhesions, cytoskeletal contractility and stem cell differentiation. Furthermore, early changes in cytoskeletal contractility predicted later stem cell fate decisions in single cells.

Cell function is regulated primarily by extracellular stimuli, including soluble and adhesive factors that bind to cell-surface receptors. Recent evidence suggests that mechanical properties of the extracellular matrix, particularly rigidity, can also mediate cell signaling, proliferation, differentiation and migration[1,2].

Culturing cells on hydrogels derived from natural extracellular matrix proteins at different densities has[3] dramatic effects on cell adhesion, morphology and function[3]. However, changing densities of the gels impacts not only mechanical rigidity but also the amount of ligand, leaving uncertainty as to the relevant contribution of these two matrix properties on the observed cellular response. Use of synthetic extracellular matrix analogs such as polyacrylamide or polyethylene glycol gels, which vary rigidity by modulating the amount of cross-linker, has revealed that substrate rigidity alone can modulate many cellular functions, including stem cell differentiation[4–6]. However, altered cross-linker amount impacts not only bulk mechanics but also molecular-scale material properties including porosity, surface chemistry, backbone flexibility and binding properties of immobilized adhesive ligands[7,8]. Consequently, whether cells transduce substrate rigidity at the microscopic scale (for example, sensing the rigidity between adhesion sites) or the nanoscopic scale (for example, sensing local alterations in receptor-ligand binding characteristics) remains an open question[7,8]. Although hydrogels will continue to be important in characterizing and controlling cell-material interactions, alternative approaches are necessary to understand how cells sense changes in substrate rigidity.

Here we report that micromolded elastomeric micropost arrays[9,10] can decouple substrate rigidity from adhesive and surface properties (**Fig. 1**). Our strategy involved a library of replica-molded arrays of hexagonally spaced poly(dimethylsiloxane) (PDMS) microposts from microfabricated silicon masters, which presented the same surface geometry but different post heights
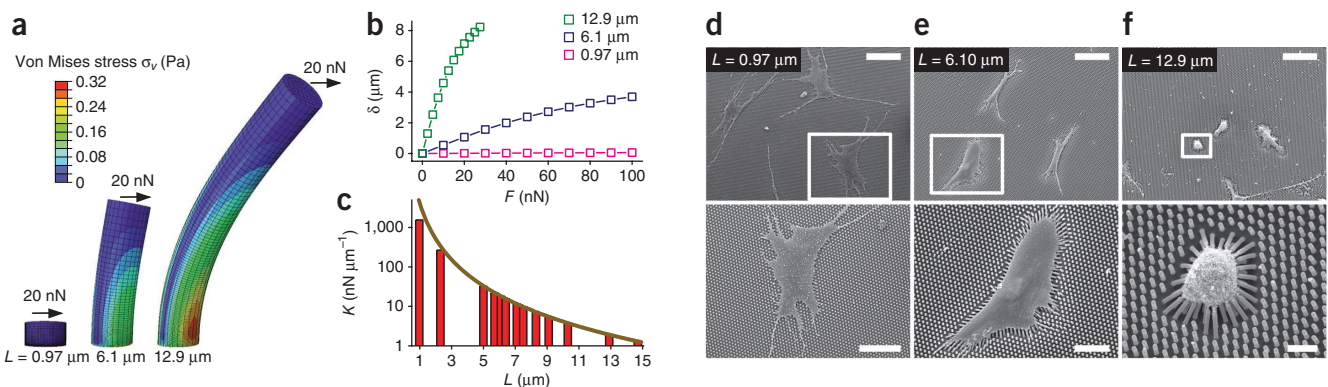

Figure 1 | Micromolded elastomeric micropost arrays to engineer substrate rigidity. (**a**) Graphical depiction of finite-element method (FEM) analysis of microposts of heights (L) each bending in response to applied horizontal traction force (F) of 20 nN. (**b**) Micropost deflection δ is plotted as a function of F, as calculated by FEM analysis. (**c**) Nominal spring constant (K) as a function of L, as computed from FEM analysis (bars) and from the Euler-Bernoulli beam theory (curve). K measures micropost rigidity. (**d**–**f**) Scanning electron micrographs of hMSCs plated on PDMS micropost arrays of the indicated heights. Images at the bottom are magnifications of the boxed regions in the top images. Scale bars, 100 μm (**d**–**f**, top), 50 μm (**d**, bottom), 30 μm (**e**, bottom) and 10 μm (**f**, bottom).

[1]Department of Bioengineering, University of Pennsylvania, Philadelphia, Pennsylvania, USA. [2]Present addresses: Department of Mechanical Engineering and Department of Biomedical Engineering, University of Michigan, Ann Arbor, Michigan, USA (J.F.) and Skeletal-Joint Research Center, National Cheng-Kung University Medical School, Tainan, Taiwan (Y.-K.W.). [3]These authors contributed equally to this work. Correspondence should be addressed to C.S.C. (chrischen@seas.upenn.edu).
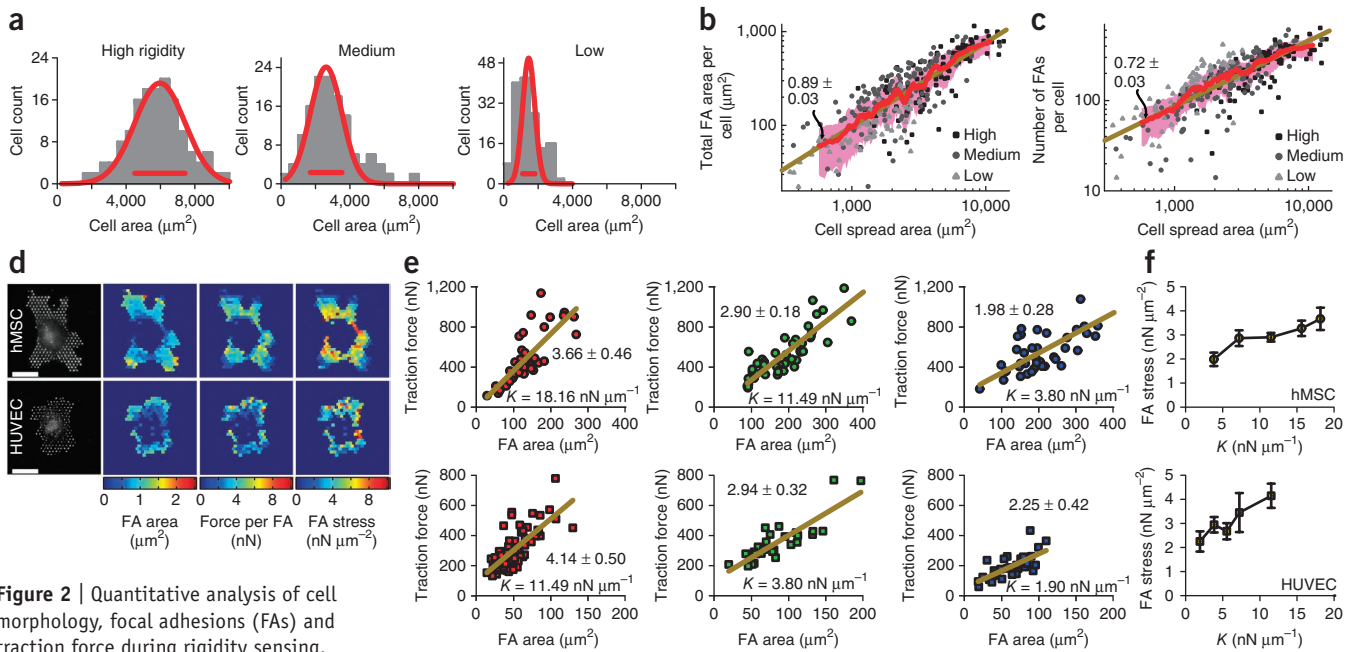
Figure 2 | Quantitative analysis of cell morphology, focal adhesions (FAs) and traction force during rigidity sensing. (**a**) Distributions of cell area for hMSCs plated on micropost arrays of different rigidities (high rigidity: $L = 0.97$ µm, $K = 1,556$ nN µm^{-1}; medium rigiditiy: $L = 6.1$ µm, $K = 18.16$ nN µm^{-1}; low rigidity: $L = 12.9$ µm, $K = 1.90$ nN µm^{-1}). Gaussian functions (red curves) were used for fitting. Red bars are centered on the mean and indicate peak widths. (**b,c**) Total FA area (**b**) and total number of FA sites (**c**) per hMSC plotted against hMSC area, for three different micropost arrays as indicated. Each data point represents an individual cell (322 cells were anlayzed). Data trends are plotted as Gaussian-weighted moving averages (red curves) ± one s.d. (pink regions) and are compared with the linear least square fitting (dark yellow lines, slope values are indicated). (**d**) Immunostaining images of FAs (left) with corresponding colorimetric maps of FA area, traction force per FA and FA stress for an hMSC and a HUVEC plated on the micropost arrays. Scale bars, 30 µm. (**e**) Traction force per single cell plotted as a function of FA area per single cell, for hMSCs (top) and HUVECs (bottom) plated on micropost arrays of different rigidities. Each data point represents an individual cell. Linear least square fits are plotted as dark yellow lines with slope values indicated. (**f**) FA stress as determined by slope values of the linear least square fits in **e** plotted against micropost rigidity K, for hMSCs (top) and HUVECs (bottom). Error bars, s.e.m.

to control substrate rigidity (**Supplementary Fig. 1** and Online Methods). Post height determines the degree to which a post bends in response to a horizontal traction force. We characterized micropost rigidity by computing the nominal spring constant, K, using the finite element method (**Fig. 1a–c**). The library of micropost arrays spanned a more than 1,000-fold range of rigidity from 1.31 nN µm^{-1} up to 1,556 nN µm^{-1}. This micropost array library is available to researchers in other laboratories (http://www.seas.upenn.edu/~chenlab/micropostform.html).

Human mesenchymal stem cells (hMSCs) have previously been shown to respond to microenvironmental cues[6,11]. We examined how hMSCs cultured on micropost arrays would respond to changes in micropost rigidity. On rigid microposts, hMSCs were well spread (**Fig. 1d**) with prominent, highly organized actin stress fibers and large focal adhesions (**Supplementary Fig. 2**). In contrast, cells on soft microposts had a rounded morphology with prominent microvilli (**Fig. 1f**), disorganized actin filaments and small adhesion complexes (**Supplementary Fig. 2**). Morphometric analysis of cell populations revealed a strong correlation between focal adhesions and cell spreading, regardless of micropost rigidity (**Fig. 2a–c**). We also observed a strong correlation between traction force and cell spreading, with a substantially smaller independent effect of micropost rigidity on traction force (**Supplementary Fig. 3**). Overall, these observations suggested that cell shape, focal adhesion structures and cytoskeletal tension were tightly coupled systems involved in rigidity sensing. The responses were similar to those reported on hydrogels of varying rigidities, but our data

suggest that rigidity sensing occurred at a micrometer scale, likely between focal adhesions because the nanoscale mechanics at the top of individual microposts (which could directly impact adhesion receptor binding) remain unchanged.

Another advantage of micropost arrays over hydrogels was that measured subcellular traction forces could be attributed directly to focal adhesions. This enabled us to map traction forces to individual focal adhesions and spatially quantify subcellular distributions of focal-adhesion area, traction force and focal-adhesion stress (defined as the ratio of traction force to corresponding focal adhesion area) (**Fig. 2d**). Although previous studies have suggested the existence of smaller focal adhesions experiencing greater stresses[12], it remains unclear how these focal adhesions are spatially organized. We observed that focal-adhesion stress was not uniform across single hMSCs. Stresses on interior focal adhesions were noticeably higher compared to those exerted on peripheral ones. This anisotropic distribution of focal-adhesion stress appeared to result from both enhanced traction force in the interior and larger focal adhesions at the periphery. A similar analysis for human umbilical vascular endothelial cells (HUVECs) revealed a distinct pattern, with both enhanced traction forces and large focal adhesions at the periphery, leading to a relatively uniform focal-adhesion stress distribution (**Fig. 2d**). Average focal-adhesion stress per cell increased with micropost rigidity for both hMSCs and HUVECs but to different magnitudes for the two cell types (**Fig. 2e,f**). These differences in focal adhesion stress between cell types suggest that there may be multiple ways for cells to mechanically adapt to their environment.

To investigate whether micropost rigidity could regulate stem cell lineage commitment, we plated hMSCs on micropost arrays with different post heights, L, and exposed them to either growth medium or bipotential differentiation medium supportive of both osteogenic and adipogenic fates[11,13]. hMSCs cultured in growth medium did not express differentiation markers at any micropost rigidity (**Supplementary Fig. 4**). In contrast, after a two week induction in bipotential differentiation medium, we observed substantial osteogenic and adipogenic differentiation on micropost arrays, indicated by alkaline phosphatase (ALP) activity and formation of

lipid droplets (Lip), respectively[11,13] (**Fig. 3a–c**). Micropost rigidity shifted the balance of hMSC fates: osteogenic lineage was favored on rigid micropost arrays whereas adipogenic differentiation was enhanced on soft ones.

To confirm these histological studies, we used quantitative real-time PCR to detect changes in gene expression of osteogenic and adipogenic markers[14,15] (**Supplementary Fig. 4c,d**); these studies were consistent with the histological data. Thus, micropost rigidity switched hMSCs between osteogenic and adipogenic lineages. The mechanism by which this rigidity-dependent switch occurred is not
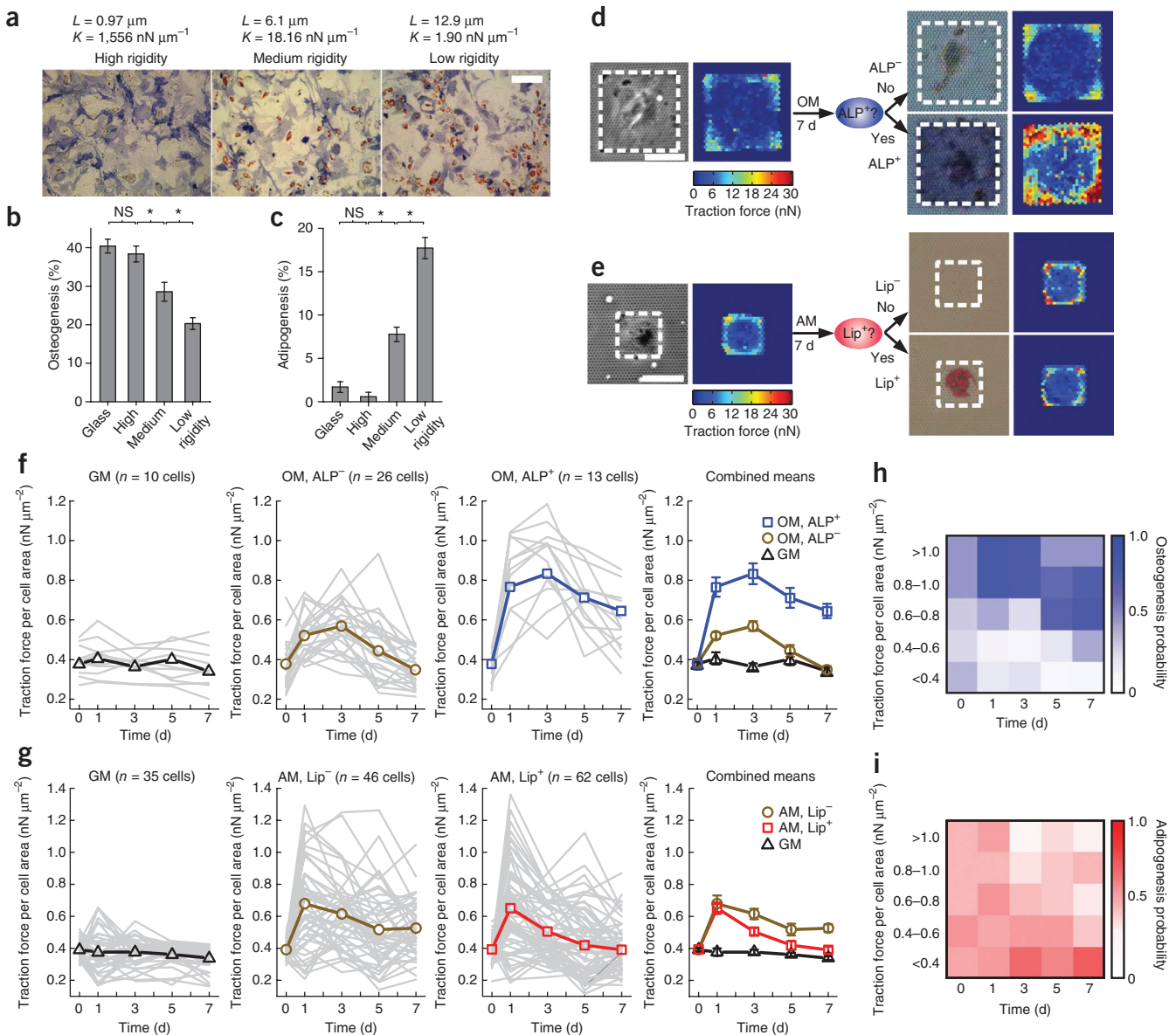

Figure 3 | Micropost arrays regulate and predict hMSC differentiation. (**a**) Brightfield micrographs of hMSCs stained for ALP and Lip after 14 d of culture in bipotential differentiation medium (MM) on micropost arrays of indicated rigidities. Scale bar, 300 μm. (**b,c**) Mean percentages of hMSC osteogenesis (**b**) and adipogenesis (**c**) as a function of micropost rigidity. Glass served as a control. Error bars, s.e.m. ($n \geq 3$). NS, not significant ($P > 0.05$), *$P < 0.05$; Student's *t*-test. (**d,e**) Brightfield micrographs and corresponding traction force maps of micropatterned single hMSCs exposed to osteogenic differentiation medium (OM; **d**) or adipogenic medium (AM; **e**) for 7 d, and then stained for ALP (**d**) or Lip (**e**). White rectangles in micrographs highlight cell boundaries. Scale bars, 50 μm. (**f,g**) Evolution of traction forces (normalized to cell area) for individual micropatterned hMSCs (thin gray lines) and population means (heavy lines) under different culture conditions as indicated. Staining is either for ALP (**f**) or Lip (**g**). Cells were grouped by medium treatment (growth medium (GM), OM or AM) and histological staining outcome (ALP+, ALP−, Lip+ or Lip−). Error bars, s.e.m. (**h,i**) Probability of differentiation of single hMSCs toward either osteogenesis (**h**) or adipogenesis (**i**) as a function of traction force (normalized to cell area) at indicated times.

yet fully understood. It is likely that the observed effects of rigidity on cell shape and cytoskeletal contractility (**Fig. 2**) are involved, as we have previously shown[11].

It also remains unclear whether endogenous cytoskeletal contractility of individual hMSCs is predictive of differentiation. Uniquely, the micropost system can be used to track traction forces of individual cells and longitudinally pair those measurements to an endpoint response measured for the same cells. We patterned single hMSCs on isolated adhesive islands of microposts, which not only restricted direct cell-cell interactions and homogenized cell shape but also permitted tracking of individual cells without the added difficulty of accounting for cell migration. We exposed the hMSCs patterned on large islands to growth medium or osteogenic differentiation medium and exposed cells on small islands to growth medium or adipogenic induction medium. We assayed live traction forces every other day for 7 d. On day 7, we assayed commitment of single hMSCs to osteogenic or adipogenic lineage by staining for ALP and Lip, respectively (**Fig. 3d,e**). We observed a strong correlation between traction forces and the ultimate differentiation status of individual hMSCs: in osteogenic differentiation medium, hMSCs that underwent osteogenic differentiation (ALP⁺) demonstrated higher traction forces than the nondifferentiating cells (ALP⁻) or the growth medium–treated controls; in adipogenic induction medium, hMSCs that did not differentiate into adipocytes (Lip⁻) were more contractile than either differentiating cells (Lip⁺) or growth medium–treated control. Although these differences in hMSC commitment were only apparent after one week of induction, heterogeneities in traction force responses emerged substantially earlier (**Fig. 3f,g**). Treatment with osteogenic differentiation medium led to upregulation of sustained traction forces as early as day 1 for hMSCs that would ultimately become ALP⁺ at day 7 (**Fig. 3f**). Adipogenic induction also upregulated traction force for both differentiating and nondifferentiating hMSCs after only 1 d of exposure (**Fig. 3g**), but this decayed rapidly after day 1, particularly in cells that ultimately committed to the adipogenic fate (Lip⁺).

Our data (**Fig. 3d–g**) suggested that there might be a window of early cytoskeletal responses critical for the later differentiation response. To test this possibility, we treated hMSCs with the reversible Rho kinase inhibitor, Y-27632 (ref. 12), for different durations during osteogenic differentiation (**Supplementary Fig. 5**). Brief treatments of hMSCs with Y-27632 for either 12 h or 1 d decreased hMSC osteogenesis at day 7. Thus, our studies revealed the importance of very early cytoskeletal responses in the hMSC differentiation process.

To investigate the predictive power of the evolution of traction forces for fate decisions of hMSCs at the single cell level, we performed Bayesian classifier analysis (**Fig. 3h,i**, **Supplementary Fig. 6** and **Supplementary Note 1**). The posterior probability, P_p, of the highly contractile hMSCs ($f = F/A > 0.8$, in which F/A is the traction force, F, normalized by cell spread area, A) in osteogenic differentiation medium at either day 1 or day 3 becoming ALP⁺ cells by day 7 ($P_p(ALP^+|f_{day\,1} > 0.8) = 0.81$ and $P_p(ALP^+|f_{day\,3} > 0.8) = 0.77$) were substantially greater than the basal prior probability for osteogenesis, $P_{Osteo}(ALP^+) = 0.33$. Similar analysis revealed that the least contractile hMSCs by days 1 and 3 ($P_p(Lip^+|f_{days\,1,3} < 0.4) = 0.87$) or days 1, 3 and 5 ($P_p(Lip^+|f_{days\,1,3,5} < 0.4) = 0.96$) were more likely to commit to adipogenesis in adipogenic

induction medium by day 7 as compared to the basal probability for adipogenesis, $P_{Adipo}(Lip^+) = 0.57$ (**Supplementary Fig. 6**). These data showed that commitment of hMSCs in single cells could be predicted a priori by monitoring the evolution of their contractile states. Such early, noninvasive predictors of cell-fate decisions might have utility in accelerating stem-cell differentiation studies, for example, in the context of drug screening, diagnostics and regenerative medicine. These early variations in mechanical responses also suggested that subpopulations of hMSCs either were predetermined or rapidly developed distinct developmental potentials, which highlights the need for deeper understanding of the subtle layers of heterogeneity in cell populations.

METHODS

Methods and any associated references are available in the online version of the paper at http://www.nature.com/naturemethods/.

Note: Supplementary information is available on the Nature Methods website.

AUTHOR CONTRIBUTIONS

J.F. and C.S.C. conceived and initiated project. J.F. and M.T.Y. designed and fabricated micropost arrays. J.F., Y.-K.W., M.T.Y., R.A.D., X.Y. and Z.L. designed and performed experiments, analyzed data and wrote the manuscript. C.S.C. supervised the project.

1. Discher, D.E., Janmey, P. & Wang, Y.-L. *Science* **310**, 1139–1143 (2005).
2. Vogel, V. & Sheetz, M. *Nat. Rev. Mol. Cell Biol.* **7**, 265–275 (2006).
3. Ingber, D.E. *Circ. Res.* **91**, 877–887 (2002).
4. Pelham, R.J. & Wang, Y.-L. *Proc. Natl. Acad. Sci. USA* **94**, 13661–13665 (1997).
5. Paszek, M.J. *et al. Cancer Cell* **8**, 241–254 (2005).
6. Engler, A.J., Sen, S., Sweeney, H.L. & Discher, D.E. *Cell* **126**, 677–689 (2006).
7. Houseman, B.T. & Mrksich, M. *Biomaterials* **22**, 943–955 (2001).
8. Keselowsky, B.G., Collard, D.M. & Garcia, A.J. *Proc. Natl. Acad. Sci. USA* **102**, 5953–5957 (2005).
9. Tan, J.L. *et al. Proc. Natl. Acad. Sci. USA* **100**, 1484–1489 (2003).
10. Yang, M.T., Sniadecki, N.J. & Chen, C.S. *Adv. Mater.* **19**, 3119–3123 (2007).
11. McBeath, R., Pirone, D.M., Nelson, C.M., Bhadriraju, K. & Chen, C.C. *Dev. Cell* **6**, 483–495 (2004).
12. Beningo, K.A., Dembo, M., Kaverina, I., Small, J.V. & Wang, Y.-L. *J. Cell Biol.* **153**, 881–888 (2001).
13. Pittenger, M.F. *et al. Science* **284**, 143–147 (1999).
14. Aubin, J.E. *Biochem. Cell Biol.* **76**, 899–910 (1998).
15. Rosen, E.D. & Spiegelman, B.M. *Annu. Rev. Cell Dev. Biol.* **16**, 145–171 (2000).

ONLINE METHODS

Design and fabrication of PDMS micropost arrays. In previous studies we characterized different fabrication approaches and specific geometries in a variety of applications and cell types[9,10]; now we used those data to develop the design parameters for mass-production of the elastomeric PDMS micropost arrays. Based on the Euler-Bernoulli beam theory approximation, we fabricated silicon micropost arrays with a post diameter of about 2 μm and heights of 1–12 μm. These post diameter and heights enabled us to obtain PDMS microposts with straight sidewalls and a broad range of rigidities to which hMSCs and HUVECs appeared to respond. The center-to-center spacing between the microposts was 4 μm, regardless of the micropost heights. This spacing between the microposts was small enough to have a minimal effect on normal cell adhesion and function but large enough to prevent adjacent microposts from collapsing into each other owing to post bending from cellular traction forces. The PDMS micropost arrays reported here had a post diameter, d, of 1.83 μm and post heights, L, ranging from 0.97 to 14.7 μm, which resulted in a more than 1,000-fold range of rigidity from 1.31 nN μm^{-1} ($L = 14.7$ μm) up to 1,556 nN μm^{-1} ($L = 0.97$ μm).

Conventional high-resolution photolithography and deep reactive ion-etching (DRIE) techniques were used to achieve batch fabrication of a large volume of silicon micropost array masters[16] (**Supplementary Fig. 1a**). A 5× reduction step-and-repeat projection stepper (Nikon NSR2005i9, Nikon Precision Inc.) was used for patterning photoresist. DRIE was performed with an inductively coupled plasma deep reactive-ion etcher (ICP Deep Trench Etching Systems, Surface Technology Systems). Heights of the microposts were controlled by varying etching time during DRIE. After stripping photoresist with Piranha solution (4:1 H_2SO_4/H_2O_2), the dimensions of the silicon microposts were measured by surface profilometry (Prometrix P-10, KLA-Tenco Co.) and scanning electron microscopy (JEOL6320FV; JEOL USA, Inc.). Finally, the silicon masters were silanized with (tridecafluoro-1,1,2,2,-tetrahydrooctyl)-1-trichlorosilane (United Chemical Technologies) for 4 h under vacuum to aid subsequent release of the negative PDMS (Sylgard 184; Dow-Corning) template from the silicon masters.

The elastomeric micropost arrays were generated with PDMS by replica-molding as previously described[10]. Briefly, to make a template containing an array of holes, PDMS prepolymer was poured over the silicon micropost masters, cured at 110 °C for 20 min, peeled off, oxidized with air plasma (Plasma Prep II; SPI Supplies) and silanized with (tridecafluoro-1,1,2,2,-tetrahydrooctyl)-1-trichlorosilane vapor overnight under vacuum. To generate the final PDMS micropost arrays, PDMS prepolymer was poured over the template, degassed under vacuum, cured at 110 °C for 20 h and peeled off the template. When peeling induced collapse of the PDMS micropost arrays, we regenerated the arrays by sonication in 100% ethanol for 30 s followed by dry-release with liquid CO_2 using a critical point dryer (Samdri-PVT-3D, Tousimis).

Finite element method characterization of nominal spring constant of PDMS microposts. The commercial finite element package ABAQUS (SIMULIA, Dassault Systèmes) was used to analyze deflections of the PDMS microposts under different applied horizontal traction forces (**Fig. 1a**). The PDMS micropost was modeled as a neohookian hyperelastic cylinder with a Young's

modulus, E, of 2.5 MPa and was discretized into hexahedral mesh elements. The bottom surface of the micropost was assigned fixed boundary conditions. A horizontal load F was then applied uniformly at all of the nodes on the top surface of the micropost. Values of Von Mises stress, σ_v, were calculated and plotted ($\sigma_v = 0.707 \times ((\sigma_1 - \sigma_2)^2 + (\sigma_2 - \sigma_3)^2 + (\sigma_1 - \sigma_3)^2)^{1/2}$, where σ_1, σ_2 and σ_3 were the principle stresses in orthogonal directions) (**Fig. 1a**). Finite-element method (FEM) analysis was performed to determine displacement, δ, of the center node on the top surface of the post owing to F. From the force-displacement curve (**Fig. 1b**), the nominal spring constant K of the PDMS micropost was determined by linearly extrapolating F to zero post deflection δ and then computing $K = dF / d\delta (\delta \rightarrow 0)$. We compared the FEM calculations of K as a function of L, with the Euler-Bernoulli beam theory approximation where $K = 3\pi Ed^4 / (64L^3)$ (**Fig. 1c**). Although the Euler-Bernoulli theoretical predictions compared well with the FEM analysis for L greater than 5 μm, the theoretical results deviated from the FEM analysis for shorter microposts. We therefore used the values of K computed from the FEM analysis for the remainder of this study.

Cell culture and reagents. Human mesenchymal stem cells (hMSCs; Lonza) were maintained in growth medium consisting of low-glucose Dulbecco's modified Eagle's medium (DMEM, Invitrogen) supplemented with 10% FBS (Atlanta Biological), 0.3 mg ml^{-1} L-glutamine, 100 units ml^{-1} penicillin and 100 μg ml^{-1} streptomycin. Early passages of hMSCs were used in experiments (passages 3–6). HUVECs (Lonza) were grown in EGM-2 (Lonza) and were maintained on gelatin-coated tissue culture polystyrene. Fresh 0.005% (vol/vol) trypsin-EDTA in PBS was used to resuspend HUVECs. For hMSC differentiation assays, hMSCs were exposed to osteogenic differentiation medium (Lonza), adipogenic induction medium (Lonza) or mixed differentiation medium (MM) consisting of a 1:1 ratio of osteogenic differentiation medium and adipogenic induction medium. Culture media were replaced every 3 d in all experiments. Aphidicolin (0.5 μg ml^{-1}; Sigma-Aldrich) was applied with every medium change to inhibit hMSC proliferation in single hMSC differentiation assays (**Fig. 3**). To block cytoskeletal contractility, ROCK inhibitor Y-27632 (10 μM; Tocris Bioscience) was applied with every medium change (**Supplementary Fig. 5**). MM was used in the experiments shown in **Figure 3** as a bipotential differentiation medium supportive of both osteogenic and adipogenic fates to investigate whether micropost rigidity could regulate the lineage commitment and differentiation of hMSCs. As osteogenesis occurs in well-spread cells but adipogenesis occurs in unspread contexts[11], it was not possible to induce both fates in sufficient numbers for patterned single hMSCs cultured in MM (data not shown). Therefore in the experiments shown in **Figure 3**, patterned single hMSCs were exposed to osteogenic differentiation medium and adipogenic induction medium for osteogenesis and adipogenesis, respectively.

Culture of (patterned) cells on PDMS micropost arrays. PDMS micropost arrays were prepared for cell attachment using microcontact printing as previously described[17]. Briefly, to generate the stamps for patterned microcontact printing, a prepolymer of PDMS was poured over a photolithographically generated SU-8 master (Microchem) on a silicon wafer. Stamps were immersed

in a saturating concentration of 50 µg ml^{-1} fibronectin (BD Biosciences) in distilled water for 1 h, washed three times in distilled water and blown dry under nitrogen. Fibronectin-coated stamps were placed in conformal contact with UV ozone–treated, surface-oxidized PDMS micropost arrays (ozone cleaner; Jelight), to facilitate fibronectin transfer from the stamp to the PDMS micropost array. PDMS micropost arrays were labeled with 5 µg ml^{-1} of Δ^9-DiI (Invitrogen) in distilled water for 1 h. After microcontact printing, protein adsorption to all PDMS surfaces not coated with fibronectin was prevented by incubating in 0.1–1% Pluronics F127 NF (BASF) in distilled water for 30 min at room temperature. hMSCs and HUVECs were seeded in growth medium onto the PDMS micropost arrays and then allowed to spread overnight before other assays were performed.

Fibronectin was used in this study primarily because of its convenience and broad applications in different surface treatments. Collagen type I was also tested and resulted in comparable results for hMSC differentiation (data not shown). Microcontact printing has proven efficient in completely transferring adhesive proteins from one surface to the other. Owing to the nature of this method, the density of the adhesive molecules on the tops of the PDMS microposts is independent of the micropost heights. Using fluorophore-labeled proteins, we compared fluorescence intensity on the tops of the microposts with different heights. No apparent difference in fluorescence intensity was observed, indicating constant protein densities on the micropost tops.

Cell staining and scanning electron microscopy specimen preparation. For F-actin visualization, cells were fixed with 4% paraformaldehyde (Electron Microscopy Science) in PBS. F-actin was detected with fluorophore-conjugated phalloidin (Invitrogen). Immunofluorescence staining of focal adhesions was performed as previously described[17]. In brief, cells were incubated in ice-cold cytoskeleton buffer (50 mM NaCl, 150 mM sucrose, 3 mM MgCl$_2$, 1 µg ml^{-1} aprotinin, 1 µg ml^{-1} leupeptin, 1 µg ml^{-1} pepstatin and 2 mM PMSF) for 1 min, followed by 1 min in cytoskeleton buffer supplemented with 0.5% Triton X-100 (Roche). Detergent-extracted cells were fixed in 4% paraformaldehyde in PBS, washed with PBS, incubated with a primary antibody to vinculin (Sigma-Aldrich) and detected with fluorophore–conjugated, isotype-specific secondary antibodies to IgG (Invitrogen).

hMSCs were fixed with 4% paraformaldehyde in PBS and stained for alkaline phosphatase using Fast Blue RR salt/naphthol (Sigma-Aldrich) per manufacturer instructions. To stain lipid fat droplets, cells were fixed in 4% paraformaldehyde, rinsed in PBS and 60% isopropanol, stained with 3 mg ml^{-1} Oil Red O (Sigma-Aldrich) in 60% isopropanol and rinsed in PBS. For total cell counts, cell nuclei were stained with 4,6-diamidino-2-phenylindole (DAPI; Invitrogen).

Scanning electron microscopy for cell culture samples was carried out at the Cell and Developmental Biology Microscopy Core at the school of Medicine of the University of Pennsylvania. Samples were washed three times with 50 mM Na-cacodylate buffer (pH 7.3; Sigma-Aldrich), fixed for 1 h with 2% glutaraldehyde (Electron Microscopy Science) in 50 mM Na-cacodylate buffer, and dehydrated in a graded series of ethanol concentrations through 100% over a period of 1.5 h. Dehydration in 100% ethanol was performed three times. After washing with 100% ethanol, dehydrated substrates were dried with liquid CO$_2$ using the super critical point dryer. Substrates were mounted on stubs and sputter-coated with gold palladium. Samples were observed and photographed using a Philips XL20 scanning electron microscope (FEI).

Real-time PCR analysis. Total RNA was isolated from hMSCs grown on the PDMS micropost arrays using RNeasy Micro kit as specified by the manufacturer (Qiagen). A total of 0.5 µg of total RNA was reverse-transcribed with MMLV reverse transcriptase (Invitrogen). Real-time PCR was performed and monitored using an ABI 7300 system (Applied Biosystems). The PCR master mixture was based on AmpliTaq Gold DNA polymerase (Applied Biosystems), and the targets were assessed using commercially available primers and probes (ALP, Hs01029144_m1; BSP, Hs00173720_m1; FrzB, Hs00989812_m1; CEBP/α, Hs00269972_s1; LPL, Hs00173425_m1; PPARγ, Hs00234592_m1; RUNX2, Hs00231692_m1; OPN (SPP1), Hs00167093_m1; Applied Biosystems). PCR was also performed with human *GAPDH* primers (Hs99999905_m1; Applied Biosystems) to detect the endogenous control for relative quantifications. Data analysis was performed using the ABI Prism 7300 Sequence Detection Systems version 1.0 software (Applied Biosystems).

Quantitative analysis of cell spread area and focal adhesions. Quantitative microscopy of focal adhesion (FA) proteins was performed using a Peltier-cooled monochrome charge-coupled device (CCD) camera (AxioCam HRM) attached to an inverted microscope (Zeiss Axiovert 200M; Carl Zeiss MicroImaging) with 20× (0.75 numerical aperture (NA); Plan-APOCHROMAT) and 40× (1.3 NA, oil immersion; EC Plan NEOFLUAR) objectives. Images were obtained using Axiovision (Carl Zeiss MicroImaging) and were processed using a custom-developed Matlab (Mathworks) program. To determine spread area for each cell, a black and white cell image was generated from the image overlay of fluorescently stained F-actin and vinculin, and the resultant white pixels were summed to quantify cell area. Briefly, the Canny edge detection method was used to binarize the actin fibers and FAs, and then image dilation, erosion and fill operations were used to fill in the gaps between the white pixels. To quantify FA number and area for each cell, the grayscale vinculin image was thresholded to produce a black and white FA image from which the white pixels, representing FAs, were counted and summed.

Quantification of traction forces. Quantitative analysis of subcellular level traction forces was performed as previously described[10,11]. Briefly, the micromolded PDMS micropost arrays underlying cells were imaged with a 40×, 1.3 NA, oil-immersion objective (EC Plan NEOFLUAR) and a CCD camera (AxioCam HRM) attached to an inverted microscope (Zeiss Axiovert 200M). The microscope was enclosed in a live cell incubator (*In vivo* Scientific) to maintain the experimental environment at 37 °C and 5% CO$_2$. For each cell, fluorescent images of the Δ^9-DiI-stained PDMS microposts were acquired at two different focal planes. The top image was acquired at the focal plane passing through the top surfaces of the microposts and the bottom one ~1 µm above the base of the microposts. These two images were analyzed with a custom-developed Matlab program to calculate traction forces. The centroids of the cross sections of the microposts in both the top and bottom images were determined by the localized

thresholding algorithm (LT) described previously[11]. Briefly, 'windows' were drawn that enclosed a single post. The region of the image within each window was converted to black and white using thresholding until the sum of white pixels that comprise the post reached the expected size of the post cross-sectional area. The centroid was then calculated from the thresholded image. Owing to the close spacing of the microposts, two-dimensional (2D) Gaussian curve fitting was used to refine the centroids calculated by the LT method, particularly for strongly deflected PDMS posts, as described previously[11]. Briefly, the grayscale intensity profile of a PDMS micropost was modeled as 2D Gaussian fits, and the centroid was determined by a nonlinear least-squares fit to this model. The top and bottom centroids calculated by these two methods represent the deflected and undeflected positions of the microposts, respectively. Using undeflected 'free' posts as reference points, the top and bottom grid of post centroids were aligned to determine the deflections, δ, for the 'attached' posts, which were then converted to the horizontal traction forces by multiplying the nominal spring constant K calculated from the FEM simulations.

16. Madou, M. *Fundamentals of Microfabrication* 1st edn. (CRC Press, New York, USA, 1997).
17. Pirone, D.M. *et al. J. Cell Biol.* **174**, 277–288 (2006).